Computational Study of the Factors Controlling Enantioselectivity in Ruthenium(II) Hydrogenation Catalysts

ARTICLE *in* INORGANIC CHEMISTRY · MAY 2008

Impact Factor: 4.76 · DOI: 10.1021/ic701981v · Source: PubMed

6 AUTHORS, INCLUDING:

Di Tommaso Devis
Queen Mary, University of London
34 PUBLICATIONS **554** CITATIONS
SEE PROFILE

Samuel Arthur French
Johnson Matthey
59 PUBLICATIONS **1,548** CITATIONS
SEE PROFILE

Richard Richard A Catlow
University College London
995 PUBLICATIONS **24,774** CITATIONS
SEE PROFILE

Inorg. Chem. **XXXX**, *xx*, 0

Inorganic Chemistry
Article

Computational Study of the Factors Controlling Enantioselectivity in Ruthenium(II) Hydrogenation Catalysts

Devis Di Tommaso,*,†,‡ **Samuel A. French**, **Antonio Zanotti-Gerosa**, **Fred Hancock**, **Erika J. Palin**,‡,§ **and C. Richard A. Catlow**‡,⊥

Davy Faraday Research Laboratory, Kathleen Lonsdale Building, University College of London, Gower Street, London WC1E 6BT, United Kingdom, and Christopher Ingold Laboratories, Department of Chemistry, University College of London, 20 Gordon Street, London WC1H OAJ, United Kingdom, Johnson Matthey Technology Centre, Blount's Court, Sonning Common, RG4 9NH, United Kingdom, Johnson Matthey Catalysis and Chiral Technologies, 28 Cambridge Science Park, Milton Road, Cambridge, CB4 0FP, United Kingdom

Received October 8, 2007

The reduction of prochiral ketones catalyzed by Ru(diphosphine)(diamine) complexes has been studied at the DFT-PBE level of theory. Calculations have been conducted on real size systems [*trans*-Ru(H)$_2$(*S*,*S*-dpen)(*S*-xylbinap) + acetophenone], [*trans*-Ru(H)$_2$(*S*,*S*-dpen)(*S*-tolbinap) + acetophenone] and [*trans*-Ru(H)$_2$(*S*,*S*-dpen)(*S*-xylbinap) + cyclohexyl methyl ketone] with the aim of identifying the factors controlling the enantioselectivity in Ru(diphosphine)(diamine) catalysts. The high enantiomeric excess (99%) in the hydrogenation of acetophenone catalyzed by *trans*-Ru(H)$_2$(*S*,*S*-dpen)(*S*-xylbinap) has been explained in terms of the existence of a stable intermediate along the reaction pathway associated with the (*R*)-alcohol. The formation of this intermediate is hindered with the competitive pathways, which consequently increases the activation energy for the hydrogen transfer acetophenone/(*S*)-phenylethanol reaction. For the [*trans*-Ru(H)$_2$(*S*,*S*-dpen)(*S*-tolbinap) + acetophenone] system, the lower enantioselectivity (i.e. 80%) is rationalized by the smaller differences in the activation energy between the competitive pathways which differentiate between the two diastereomeric approaches of the prochiral ketone. The DFT-PBE results suggest that this reaction is driven to the (*R*)-product only by the process of binding the acetophenone to the active site of the *trans*-Ru(H)$_2$(*S*,*S*-dpen)(*S*-tolbinap) catalyst. For the hydrogenation of cyclohexyl methyl ketone catalyzed by *trans*-Ru(H)$_2$(*S*,*S*-dpen)(*S*-xylbinap), the low performance in the enantioselective hydrogenation of the dialkyl ketone (i.e. 37%) is again explained by the small differences in the activation and binding energies which are the factors which could effectively differentiate between the two alkyl groups.

1. Introduction

Enantiomerically pure secondary alcohols are valuable intermediates for the manufacture of structurally interesting and biologically active compounds. Hence, the developments of highly effective systems for the synthesis of chiral alcohols is not only of fundamental importance but also of substantial relevance to industrial applications. One of the most significant developments in this field was the discovery by Noyori and co-workers of highly efficient Ru(II)-amine ligand based complexes for the enantioselective hydrogenation of ketones.[1] The mechanism involved in the hydrogen transfer ketone/alcohol reaction promoted by Noyori-type complexes is metal–ligand (M-L) bifunctional catalysis:[2] the ketone coordinates to the outer coordination sphere of the Ru(II)-amine complex, and it has been proposed that the hydride (Ru−)H and the protic (N−)H are transferred to the C═O functionality via a six-membered pericyclic transition state.[3]

* Author to whom correspondence should be adressed. Electronic mail: uccaddi@ucl.ac.uk.
† Present address: Department of Chemistry, Christopher Ingold Laboratories, University College of London, 20 Gordon Street, London WC1H 0AJ, United Kingdom.
‡ Davy Faraday Research Laboratory.
§ Present address: Department of Earth Sciences, University of Cambridge, Downing Street, Cambridge CB2 3EQ, United Kingdom.
⊥ Christopher Ingold Laboratories.

(1) (a) Noyori, R.; Ohkuma, T. *Angew. Chem., Int. Ed.* **2001**, *40*, 40. (b) Noyori, R. *Angew. Chem., Int. Ed.* **2002**, *41*, 2008 ; Nobel Lecture.
(2) (a) Noyori, R.; Koizumi, M.; Ishii, D.; Ohkuma, T. *Pure Appl. Chem.* **2001**, *73*, 227. (b) Noyori, R.; Kitamura, M.; Ohkuma, T. *Proc. Natl. Acad. Sci. USA* **2004**, *101*, 5356. (c) Ikariya, T; Murata, K; Noyori, R. *Org. Biomol. Chem.* **2006**, *4*, 393.
(3) Sandoval, C. A.; Ohkuma, T.; Muñiz, K; Noyori, R. *J. Am. Chem. Soc.* **2003**, *125*, 13490.

10.1021/ic701981v CCC: $37.00
Published on Web 03/05/2008

These catalysts display an exceptional degree of enantio- and chemoselectivity for the C═O group, which originates from the charge alternating arrangement in the transition state structure of the atoms involved in the H-transfer process. Experimental and several theoretical studies on model reactions[3,4] agree in revealing the M-L mechanism to be the most favorable reaction pathway. Very recently, a Car–Parrinello molecular dynamics study on a model Ru arene amino alcohol complex[5] has revealed that the proton source for the ketone may be either the solvent or the amine ligand.

Among the best catalysts for carbonyl hydrogenation developed by Noyori are ternary ruthenium complexes made up of $(\text{phosphane})_n$ and diamine and a Ru(II) center.[1] The active species is the *trans*-dihydride, which is formed by the reaction of the precursor dichloro complex with dihydrogen and alkoxy base.[3,6] Since the modular composition of the catalyst allows for selective replacement of the individual ligands, the identification of a suitable combination of the organic $(\text{phosphane})_n$ and diamine ligands is a key factor in generating high performance catalysts for asymmetric hydrogenation. In particular, the experimental evidence shows how subtle modifications of the structure of the $(\text{phosphane})_n$ can produce very significant changes in the enantioselectivity and reaction rate of the ketone hydrogenation reaction.

One of the most intriguing aspects encountered in the development of diarylphosphine ligands (such as the BINAP family of ligands[7]) is the so-called "3,5-dialkyl meta-effect": the position of the alkyl groups in the aryl substituents of the $(\text{phosphane})_n$ ligands significantly changes the enantioselectivity of the reaction. Indeed, 3,5-dialkyl substituted arene groups generally impart higher enantioselectivity to the catalyst,[8] and in the field of organometallic catalysis, this effect is one of the most important factors governing the relationship between the ligand structure and catalytic efficacy.[9]

Scheme 1

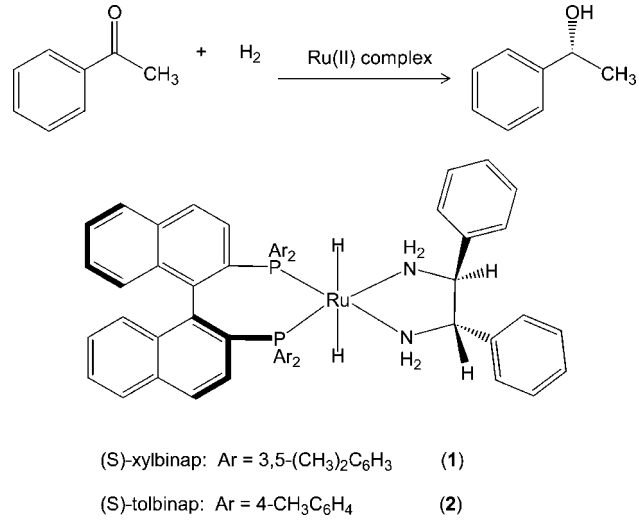

(S)-xylbinap: Ar = 3,5-$(CH_3)_2C_6H_3$ (**1**)

(S)-tolbinap: Ar = 4-$CH_3C_6H_4$ (**2**)

Therefore, understanding the origin of the 3,5-dialkyl meta-effect will certainly help in the process of rational ligand design.

Scheme 1 reports one of the most prominent examples of the 3,5-dialkyl meta-effect: acetophenone is reduced to (*R*)-phenylethanol with an enantiomeric excess (e.e.) of 99% if the reaction is catalyzed by *trans*-$Ru(H)_2$(*S*,*S*-dpen)(*S*-xylbinap) (**1**),[10] and the e.e is considerably reduced to 80% when the reaction is promoted by *trans*-$Ru(H)_2$(*S*,*S*-dpen)(*S*-tolbinap).[11] Note that the position of the methyl groups in the aryl substituents at the phosphorus atom is the only structural difference between **1** and **2** (meta position in **1**, para position in **2**), but this subtle modification in the diphosphine ligand causes a significant variation in the e.e. However, geometry optimization of the bare catalysts **1** and **2** at the density functional theory level shows that the electronic nature of the atom directly involved in the reaction [Ru−H, N−H], as well as the structural parameters of the "core" of the catalysts, do not differ between **1** and **2**.[12] Therefore, the origin of the 3,5-dialkyl meta-effect may reside not so much in changes in the transition state but rather in the "docking" of the substrate into the reactive pocket well before the bond breaking/forming interactions are established.

In a recent communication,[13] we showed that the high enantioselectivity in the hydrogenation of acetophenone

(4) (a) Alonso, D. A.; Brandt, P.; Nordin, S. J. M.; Andersson, P. G. *J. Am. Chem. Soc.* **1999**, *121*, 9580. (b) Yamakawa, M.; Ito, H.; Noyori, R. *J. Am. Chem. Soc.* **2000**, *122*, 1466. (c) Noyori, R.; Yamakawa, M.; Hashiguchi, S. *J. Org. Chem.* **2001**, *66*, 7931. (d) Abdur-Rashid, K.; Clapham, S. E.; Hadzovic, A.; Harvey, J. N.; Lough, L. J.; Morris, E. H. *J. Am. Chem. Soc.* **2002**, *124*, 15104. (e) Handgraaf, J.; Reek, J. N. H.; Meijer, E. J. *Organometallics* **2003**, *22*, 3150. (f) Brandt, P; Roth, P.; Andersson, P. G. *J. Org. Chem.* **2004**, *69*, 4885.

(5) Handgraaf, J.; Meijer, E. J. *J. Am. Chem. Soc.* **2007**, *129*, 3099.

(6) Abdur-Rashid, K.; Faatz, M.; Lough, A. L.; Morris, R. H. *J. Am. Chem. Soc.* **2001**, *123*, 7473.

(7) BINAP is 2,2′-bis. (diphenylphosphino)-1,1′-binaphthyl. (a) Miyashita, A.; Yasuda, A.; Takaya, H.; Toriumi, K.; Ito, T.; Souchi, T.; Noyori, R. *J. Am. Chem. Soc.* **1980**, *102*, 7932. (b) Takaya, H.; Akutagawa, S.; Noyori, R. *Org. Synth., Coll.* **1993**, *8*, 57.

(8) (a) Burk, M. J.; Herms, W.; Herzberg, D.; Malan, C.; Zanotti-Gerosa, A. *Org. Lett.* **2000**, *2*, 4173. (b) Wu, J.; Ji, J.; Guo, R.; Yeung, C.; Chan, A. S. C. *Chem.—Eur. J.* **2003**, *9*, 2963. (c) Ohkuma, T.; Hattori, T.; Ooka, H.; Inoue, T.; Noyori, R. *Org. Lett.* **2004**, *6*, 2681. (d) Jing, Q.; Zhang, X.; Sun, J.; Ding, K. *Adv. Synth. Catal.* **2005**, *347*, 1193. (e) Xu, Y.; Clarkson, G. C.; Doehrty, G.; North, C. L.; Woordward, G.; Wills, M. *Chem.—Eur. J.* **2005**, *70*, 8079. (f) Xie, J-H.; Liu, S.; Huo, X-H.; Cheng, X.; Duan, H-F.; Fan, B-H.; Wang, L-X.; Zhuo, Q-L. *J. Org. Chem.* **2005**, *70*, 2967. (g) Scalone, M.; Waldmeier, P. *Org. Process. Res. Dev.* **2003**, *7*, 418. (h) Ohkuma, T.; Sandoval, C. A.; Srinivasan, R.; Lin, Q.; Wei, Y.; Muniz, K.; Noyori, R. *J. Am. Chem. Soc.* **2005**, *127*, 8288.

(9) (a) Trabesinger, G.; Albinati, A.; Feiken, N.; Kunz, R. W.; Pregosin, P. S.; Tschoerner, M. *J. Am. Chem. Soc.* **1997**, *119*, 6315. (b) Dotta, P.; Magistrato, A.; Rothlisberger, U.; Pregosin, P. S.; Albinati, A. *Organometallics* **2002**, *21*, 3033.

(10) XylBINAP = 2,2′-bis-(di-3,5-xylylphosphino)-1,1′-binaphthyl. DPEN = 1,2-diphenylethylenediamine. (a) Ohkuma, T.; Koizumi, M.; Muñiz, K.; Hilt, G.; Kabuto, C.; Noyori, R. *J. Am. Chem. Soc.* **2002**, *124*, 6508. (b) Ohkuma, T; Koizumi, M.; Doucet, H.; Pham, T.; Kozawa, M.; Murata, K.; Katayama, E.; Yokozawa, T.; Ikariya, T.; Noyori, R. *J. Am. Chem. Soc.* **1998**, *120*, 13529.

(11) TolBINAP = 2,2′-bis. (di-4-tolylphosphino)-1,1′-binaphthyl. Doucet, H.; Ohkuma, T.; Murata, K.; Yokozawa, T.; Kozawa, M.; Katayama, E.; England, A. F.; Ikariya, T.; Noyori, R. *Angew. Chem., Int. Ed.* **1998**, *37*, 1703.

(12) Geometry optimization and analysis of the atomic charges performed at the PBE level. Analysis of the atomic charges performed at the B3LYP and BB1K level using the PBE optimized geometry.

(13) French, S. A.; Di Tommaso, D.; Zanotti-Gerosa, A.; Hancock, F.; Catlow, C. R. A. *Chem. Commun.* **2007**, 2381.

Scheme 2

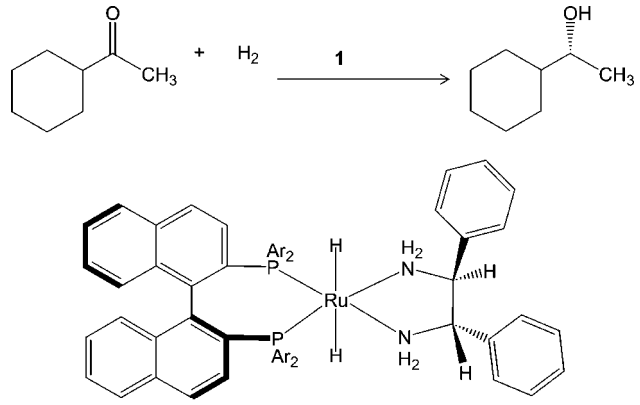

(S)-xylbinap: Ar = 3,5-$(CH_3)C_6H_3$ (1)

catalyzed by *trans*-$Ru(H)_2$(*S*,*S*-dpen)(*S*-xylbinap) can be explained by the formation of a stable intermediate along the reaction pathway associated with the (*R*)-product. In the present work, we present a detailed investigation on the electronic and steric effects that favor the formation of this stable intermediate along the (*R*)-alcohol reaction pathway while hindering it for the competitive (*S*)-pathways. Moreover, we extend the investigation to the *trans*-$Ru(H)_2$(*S*,*S*-dpen)(*S*-tolbinap)-catalyzed acetophenone hydrogenation, with the aim of understanding the factors governing the enantioselectivity in the class of catalysts reported in Scheme 1, with particular emphasis on the origin of the 3,5-dialkyl meta-effect.

To further our study of the factors controlling enantioselectivity, we consider the *trans*-$Ru(H)_2$(*S*,*S*-dpen)(*S*-xylbinap)-catalyzed cyclohexyl methyl ketone hydrogenation, which is reported in Scheme 2. Experimental evidence[14] shows that the (*R*)-alcohol is obtained with a low e.e. (19–37%), and the aim is to identify the factors that determine such a low performance. The asymmetric hydrogenation of aliphatic ketones remains a challenging problem for organometallic catalysts,[15] to which computational studies of the type reported here can make a substantial contribution.

2. Methodology

Here, we summarize the computational approach used in this study. First, we describe the density functional theory (DFT) methodology used for total energies and geometry optimization and then the strategy employed to locate the structure of the transition state for the H-transfer ketone/alcohol reaction via the metal–ligand (M-L) bifunctional mechanism.

2.1. Computational Details. The DFT calculations were performed using the DMol[3] code from Accelrys (Materials Studio 3.2).[16,17] In DMol[3] the electronic wave function is expanded in a

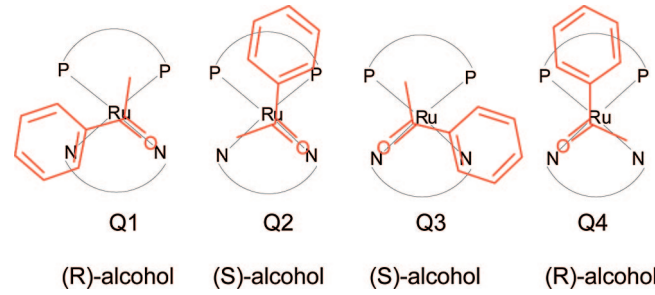

Figure 1. Definition of the possible reaction paths with the subsequent stereochemical configuration of the alcohol product.

localized atom-centered basis set with each basis function defined numerically on a dense radial grid. The inner core–electrons for Ru were represented by the DFT semilocal pseudopotential (DSPP) specifically developed for DMol[3] calculations, while sixteen electrons were treated explicitly for Ru (those corresponding to the atomic levels 4s, 4p, 4d, 5s). We used the double-numeric-polarized (DNP) basis sets, which are variationally comparable to 6-31G(d,p) basis sets. However, the numerical functions are far more complete than the traditional Gaussian functions. Because of the quality of these orbitals, basis set superposition effects are minimized[16] and it is possible to obtain an excellent description, even of weak bonds. Indeed, the numerical basis set is more spatially extended than 6-31G(d,p) basis sets and is therefore able to describe the tail of the wave function due to the long-range interaction. Each basis function was restricted to within a cutoff radius of $R_{cut} = 4.7$ Å. The electron density was approximated using a multipolar expansion up to octupole. For total energies and geometry optimization, the gradient corrected PBE[18] exchange-correlation functional was used. It is well-known that generalized-gradient-corrected (GGA) density functionals have the tendency to underestimate the activation energies. However, a systematic computational study on the hydrogen transfer acetone/*i*-propyl alcohol reaction catalyzed by a model trans-$Ru(H)_2$(diphosphine)(diamine) complex[19] showed that the forward activation barrier calculated at the PBE level differs by less than 2 kcal/mol from the result obtained using the BB1K hybrid meta GGA functional,[20] probably the best density functional type method for kinetics.[20,21]

2.2. Location of the Transition State. To investigate the selectivity of the reactions, it is necessary to compute all the different ways in which the prochiral ketone can approach to the active sites (Ru−H, N−H) of the catalysts. These different pathways are schematically classified according to the criteria in Figure 1. When the approach is Q1 or Q4, the product is the (*R*)-alcohol; when the approach is Q2 or Q3, the product is the (*S*)-alcohol. In order to study the factors controlling enantioselectivity, it is necessary to locate the structures of the transition state and intermediates along each reaction pathway. For the systems reported in Schemes 1 and 2, the localization of the six-membered transition state involved in the metal–ligand (M-L) bifunctional mechanism is a challenging task. Indeed, because of the size of the system, the traditional method involving calculation of the Hessian and

(14) $RuCl_2$(*R*,*R*-dpen)(*R*-XylBinap) reduced cyclohexyl methyl ketone at substrate to catalyst molar ratio (S/C) of 5000/1, 12% *t*-BuOK, *i*-PrOH, 30°C, 10 bar hydrogen, 18 h giving full conversion and 37% e.e.; under the same conditions, $RuCl_2$(*R*,*R*-dpen)(*R*-TolBinap) gave 19% e.e.

(15) Jiang, Q.; Jiang, Y.; Xiao, D.; Cao, P.; Zhang, X. *Angew. Chem., Int. Ed.* **1998**, *37*, 1100.

(16) (a) Delley, B. *J. Chem. Phys.* **1990**, *92*, 508. (b) Delley, B. *J. Chem. Phys.* **2000**, *113*, 7756.

(17) *DMol*[3], *Materials Studio*, version 3.2; Accelrys: San Diego, CA, http://www.accelrys.com/products/mstudio/.

(18) Perdew, J. P.; Burke, K.; Ernzerhof, M. *Phys. Rev. Lett.* **1996**, *77*, 3865.

(19) Di Tommaso, D.; French, S. A.; Catlow, C. R. A. *J. Mol. Struct.: THEOCHEM* **2007**, *812*, 39.

(20) Zhao, Y.; Lynch, J. B.; Truhlar, D. G. *J. Phys. Chem A* **2004**, *108*, 2715.

(21) (a) Zhao, Y.; Schultz, N. E.; Truhlar, D. G. *J. Chem. Theory Comput.* **2006**, *2*, 234. (b) Hemelsoet, K.; Moran, D.; Van Speybroeck, V.; Waroquier, M; Radom, L. *J. Phys. Chem. A* **2006**, *110*, 8942.

following the reaction mode is extremely costly and the success of such calculations is not guaranteed unless the initial structure is already close to the transition state. Moreover, various attempts to use methods such as the linear synchronous transit/quadratic synchronous transit (LST/QST) as implemented in the DMol^3 code for the localization of the transition state failed, owing probably to the size and complexity of the systems. However, this problem can be simplified as a result of our earlier computational study conducted on a model reaction, which has shown that, for *trans*-Ru(H)$_2$(diphosphine)(diamine) catalyzed H-transfer ketone/alcohol reactions, the (Ru−)H···C(=O) internuclear distance can be considered as the pseudo reaction coordinate for the M-L mechanism.[19] In fact, this study showed that among the internuclear distances directly involved in the hydrogen transfer reaction [i.e., Ru−H, C−H, N−H and O−H], the (Ru−)H···C(−O) distance is clearly the one that changes mostly on going from the Ru−ketone reactant complex to the transition state structure. Furthermore, the analysis of the single imaginary frequency of the computed transition clearly indicated that in the H-transfer reaction, the amplitude is largest at the C−H of the hydride between Ru and C of the carbonyl group and less extensive for the proton transfer between N and O. Note that, in this study,[19] the structures of the transition state associated with the ketone hydrogenation were obtained using LST/QST procedure followed by optimization of the transition state via the eigenvector following (EF) method as implemented in the DMol^3 code, or using the synchronous transit-guided quasi-newton (STQN) methods as implemented in the Gaussian code. Therefore, an approximate reaction path for the H-transfer process could be obtained by probing the potential energy surface (PES) with respect to the (Ru−)H···C(=O) distance. Therefore, starting from separate non interacting reactants, at each stage the geometry of the system has been optimized with respect to the constraint, namely the (Ru−)H···C(=O) distance. The output from one simulation was used to generate the initial conformation of the next. The geometry was considered to be convergent when the gradient was less than 0.002 hartree/Å and the energy change was less than 10^{-5} hartree. These calculations were performed on the real size {*trans*-Ru(H)$_2$(diphosphine)(diamine) + ketone} systems reported in Schemes 1 and 2 and for each possible approach of the ketone to the active sites of the catalyst (Q1, Q2, Q3, and Q4 in Figure 1). From the electronic energy chart, the transition state structure for the hydrogen transfer ketone/alcohol reaction (Hydrog.TS) was determined as the maximum point along the pseudo reaction coordinate (Ru−)H···C(=O) and positioned at about 2 Å. The structures corresponding to the minima in the electronic energy chart (if found) were freely optimized.

To test this approach, the harmonic vibrational frequencies were computed for the systems [**1** + cyclohexyl methyl ketone] on the structure corresponding to the maximum energy along the (Ru−)H···C(=O) distance of the Q1 approach. The vibrational analysis showed a single negative frequency corresponding mostly to the transfer of the hydride between Ru and C of the carbonyl group and less extensively to the proton transfer between N and O. This structure was optimized to the Hydrog.TS structure using the eigenvector following method[22] as implemented in DMol^3. The total energy, the internuclear distances of the "core" of the system and the imaginary frequency for the optimized and approximated Hydrog.TS of the [**1** + cyclohexyl methyl ketone] are reported in Table 1. It is possible to notice that the internuclear distances differ by less than 0.01, and the difference in the total electronic energies is just 0.80 kJ/mol. Further support for this method is provided by the similarity of the approximated Hydrog.TS of [**1** + cyclohexyl methyl ketone] with the structure of the transition states for the acetone/*i*-propyl alcohol reaction catalyzed by *trans*-Ru(H)$_2$(PH$_3$)$_2$(NH$_2$CH$_2$CH$_2$NH$_2$)[19] and *trans*-Ru(H)$_2$(PR$_2$CHCR′CR′CHPR$_2$)(NH$_2$CH$_2$CH$_2$NH$_2$) (where R, R′ = CH$_3$, Ph) model catalysts[31] obtained using the LST/QST method followed by optimization of the transition state via the eigenvector following method with the DMol^3 code.

Consequently, all the arguments presented above validate the approach used in the present work to approximate the structure of the transition state involved in the M-L bifunctional mechanism in the case of Ru(diphosphine)(diamine)-catalyzed ketone hydrogenation as the maximum of the PES along the reaction coordinate defined by the (Ru−)H···C(=O) separation.

Table 1. Total Electronic Energy (hartree), Structure (in angstroms), and Imaginary Frequency (in inverse centimeters) for the Optimized and Approximated Transition State of the Hydrogen Transfer Cyclohexyl Methyl Ketone/Cyclohexyl Methyl Alcohol Reaction Catalyzed by *trans*-Ru(H)$_2$(*S*,*S*-dpen)(*S*-xylbinap) Catalyst (**1**) As Computed by the DFT-PBE Method

	optimized Hydrog.TS	approximated Hydrog.TS
energy	−3858.4585	−3858.4582
r(Ru−N)	2.182	2.184
r(Ru−P)	2.271	2.271
r(Ru−H)	1.843	1.833
r(N−H)	1.041	1.041
r(C−H)	1.799	1.800
r(O−H)	1.864	1.867
r(C=O)	1.267	1.266
ν	−301	−232

3. Results and Discussion

3.1. Reduction of Acetophenone by *trans*-Ru(H)$_2$(*S*,*S*-dpen)(*S*-xylbinap). Figure 2 shows the variation in the calculated total energy of the system [**1** + acetophenone] as a function of the pseudo reaction coordinate (Ru−)H···C(=O) for each possible approach of acetophenone to the active sites of the catalysts (Q1, Q2, Q3, Q4). We note that no account is taken of thermal and entropic effects.

All four pathways show a maximum energy centered at approximately 2 Å along the (Ru−)H···C(=O) internuclear distance, which corresponds to the transition state structure for the hydrogen transfer acetophenone/phenylethanol reaction via the M-L mechanism (Hydrog.TS). The energies of the Hydrog.TS structures relative to that of the separated reactants (considered at 9 Å) are: −7.61 kJ/mol for Q1, 9.58

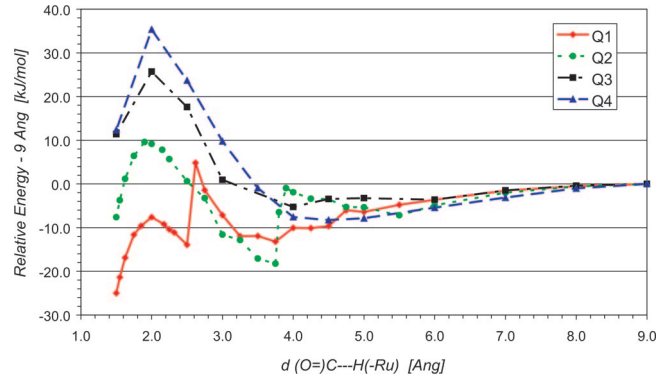

Figure 2. Electronic energy variation of the system [*trans*-Ru(H)$_2$(*S*,*S*-dpen)(*S*-xylbinap) + acetophenone] along the [(Ru−)H···C(=O)] internuclear distance for each possible approach (Q1, Q2, Q3, Q4). Values computed at the DFT-PBE level of theory.

(22) Baker, J. *J. Comput. Chem.* **1986**, *7*, 385.

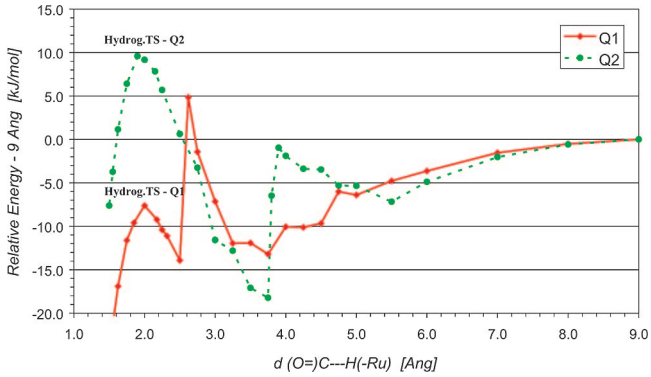

Figure 3. Electronic energy variation of the system [*trans*-Ru(H)$_2$(*S*,*S*-dpen)(*S*-xylbinap) + acetophenone] along the [(Ru−)H···C(=O)] internuclear distance for the Q1 and Q2 approaches. Values computed at the DFT-PBE level of theory.

kJ/mol for Q2, 25.70 kJ/mol for Q3, and 35.36 kJ/mol for Q4. Since the reaction will proceed through the lowest energy saddle point, it is evident that the H-transfer process is by far the most favorable along the Q1 approach, which gives the *R*-alcohol as a resulting product, in agreement with experiment.

The four alternative pathways display very different energetic trends. For the Q3 and Q4 approaches, whose Hydrog.TSs are the most unstable, no energy minima have been located along the pseudo reaction coordinate (Ru−)H···C(=O). In contrast, the variation in the energy for the acetophenone entrance in the Q1 and Q2 approaches show more interesting features, which are considered in detail in Figure 3. The Q1 approach displays an energy profile with a double-well and two distinct minima at 3.75 and 2.5 Å. For the Q2 approach, a single minimum along the pseudo reaction coordinate (Ru−)H···C(=O) has been located at 3.75 Å. The existence of two stable intermediates along the Q1 pathway is likely to stabilize its Hydrog.TS compared to the competitive Q2 approach. In order to verify this hypothesis, the two minima at 3.75 and 2.5 Å along Q1 and the minimum at 3.75 Å along Q2 have been freely optimized. For Q1 and Q2, the freely optimized minima (INT-I and INT-II for Q1, INT-I for Q2) and Hydrog.TS structures are shown in Figures 4 and 5, respectively, and described in Table 2. We first describe the optimized structures and the energetics of the intermediates and Hydrog.TS for the Q1 approach. We then present the minima and Hydrog.TS structures located along the Q2 pathway.

From Figure 4, the intermediate INT-I along Q1 corresponds to the situation where the acetophenone is outside the pocket made by the bulky aryl groups of the catalyst **1** and where the phenyl group of the acetophenone is approximately on the plane defined by the C−C=O atoms (in Table 2, $\gamma = -4.5°$). In the intermediate INT-II, the phenyl group of the acetophenone is rotated with respect to INT-I (in Table 2, γ changes from −4.5° in INT-I to 19.8° in INT-II) in order to enter into the pocket of the catalyst **1**. Moreover, Table 2 shows that the torsional angle of the phenyl group γ is the structural parameter that changes most significantly on going from INT-I to INT-II. In particular, the out-of-plane bending of the carbonyl carbon τ in INT-I

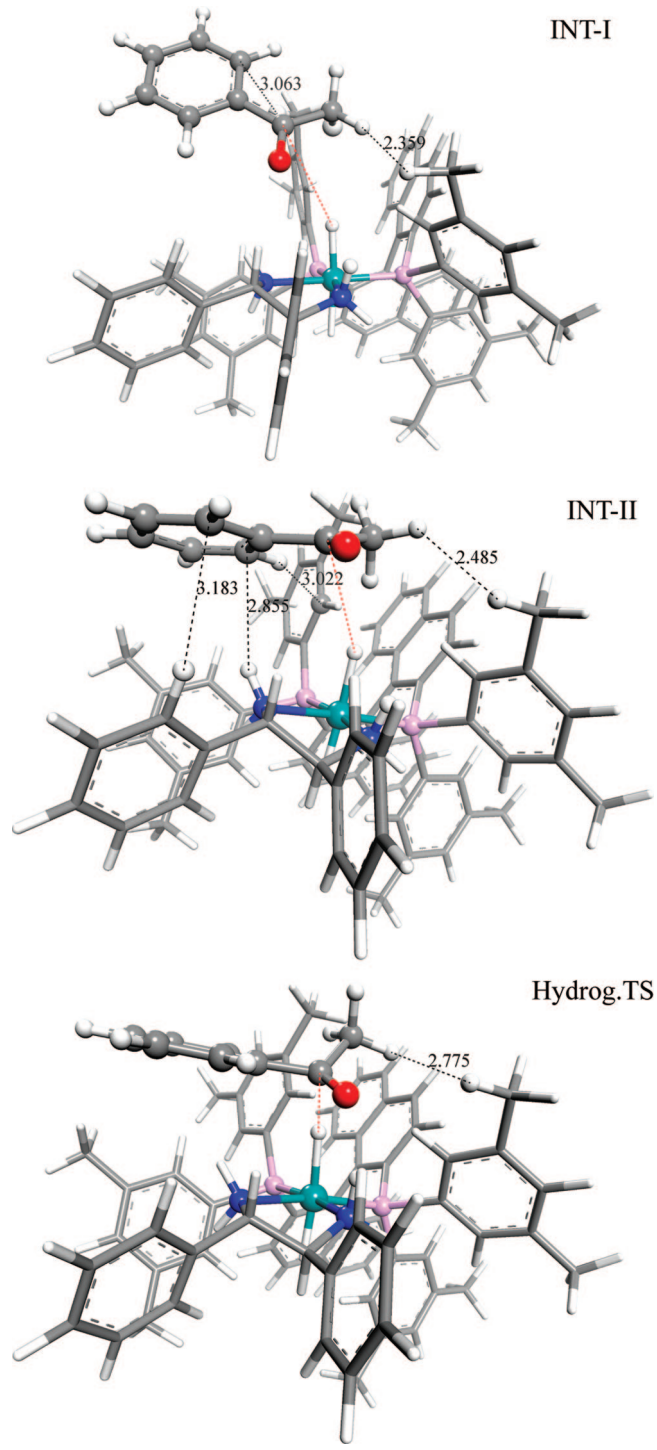

Figure 4. Minima (INT-I, INT-II) and transition-state-like (Hydrog.TS) structures for acetophenone entry in the active sites of the *trans*-Ru(H)$_2$(*S*,*S*-dpen)(*S*-xylbinap) catalyst along the Q1 pathway as computed by the DFT-PBE method.

($\tau = 1.0°$) and INT-II ($\tau = 1.1°$) indicates that the carbon still has sp^2 character in both intermediates. Along the Q1 approach, the relative energies of the intermediates indicate an extra-stabilization of ∼10 kJ/mol when the acetophenone enters into the pocket (INT-II) of the catalyst **1**. The larger stabilization of the intermediate INT-II compared to INT-I (and to the isolated acetophenone and catalyst) can be explained by electronic and steric effects.

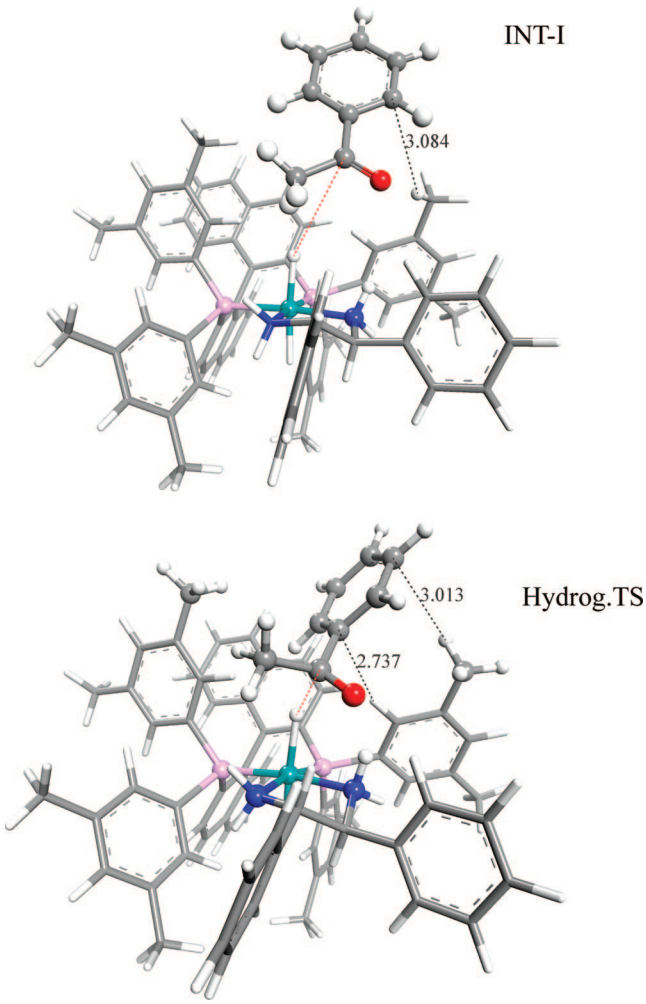

Figure 5. Minima (INT-I) and transition-state-like (Hydrog.TS) structures for acetophenone entry in the active sites of the *trans*-Ru(H)$_2$(*S*,*S*-dpen)(*S*-xylbinap) catalyst along the Q2 pathway as computed by the DFT-PBE method.

In [**1** + acetophenone], the presence of π-systems, which act as weak bases, allows the formation of XH/π (X = N and C) hydrogen bonds when the XH hydrogen donor and the aromatic π-moiety hydrogen acceptor come in close contact. These weak hydrogen bonds are the key to the extra-stabilization of INT-II. In the intermediate INT-I, we notice the occurrence of a weak C(sp^3)H/π attraction[23] as the C(sp^3)H···C(π) distance reported in Figure 4 is close to the sum of the van der Waals radii (2.95 Å[24]). The attractive interaction is indicated by the larger positive Mulliken charge of the hydrogen C(sp^3)H donor (+0.113 au) and the larger negative charge of the C(π) acceptor (−0.080 au) compared with the atomic charges computed in the separated reactants [+0.096 au for C(sp^3)H and −0.062 au for C(π)]. The conformational change of the acetophenone in INT-II enables the phenyl group to form a stronger C(sp^2)H···π interaction[23] between, for example, the acetophenone C(sp^2)H donor and the aryl moiety acceptor at a distance of 3.022 Å (see Figure 4). Indeed, the positive charge at the interacting C(sp^2)H donor (+0.133 au) is much larger than in the free acetophenone (+0.059 au) and considerably larger than in INT-I (+0.094 au). For the π acceptor, the charge of the C atom at the π acceptor (−0.035 au) is more negative than in the isolated catalyst **1** (−0.019 au). Possibly, a second C(sp^2)H···π attraction could be assigned to the atoms at the internuclear distance of 3.183 Å (see Figure 4), as the negative charge at the C atom of the π acceptor changes from −0.047 au in INT-I to −0.066 au in INT-II. More importantly, the torsion of the phenyl group in INT-II enables the N−H donor of the DPEN ligand to form a NH/π hydrogen bond[25] (which is stronger than the CH/π interaction[26]) with the C(π) atom of the acetophenone at the distance of 2.855 Å. The Mulliken charge of the (N−)H donor changes from +0.237 au in INT-I to +0.261 in INT-II, while the charge of the C(π) acceptor changes from −0.080 au in INT-I to −0.105 au in INT-II. In summary, the conformational change in INT-II, which is highlighted by the rotation of the phenyl group, enables the formation of stronger hydrogen-bond like attractive interactions between the phenyl group of the ketone and the aryl moieties of the catalyst, which stabilizes the [**1** + acetophenone] system with respect to the situation where the acetophenone is outside of the pocket (INT-I). It is worth noting that it is well-known that XH/π hydrogen bonds, while considerably weaker than classical H bonding, play notable structure-determining, structure stabilizing and selective-binding roles throughout chemistry and biology.[27]

For the Q1 approach, steric effects also play a role in the extra-stabilization of INT-II: the minimum H···H distance between the methyl group of the acetophenone and the methyl group of the aryl group in the meta position increases

(23) Nishio, M.; Hirota, M.; Umezawa, Y. *The CH/π Interaction - Evidence, Nature and Consequences*; Wiley/VCH: New York, 1998.
(24) The source of the van der Walls radii is Bondi, A. *J. Phys. Chem.* **1964**, *68*, 441 who gives values of 1.20 Å for H, 1.52 Å for O, 1.55 Å for N, and 1.75 Å for C.
(25) (a) Oki, M.; Mutai, K. *Bull. Chem. Soc. Jpn.* **1960**, *33*, 784. (b) Oki, M.; Mutai, K. *Bull. Chem. Soc. Jpn.* **1965**, *38*, 387. (c) Oki, M.; Mutai, K. *Bull. Chem. Soc. Jpn.* **1966**, *39*, 809.
(26) Tsuzuki, S.; Honda, K.; Uchimaru, T.; Mizami, M; Tanabe, K. *J. Am. Chem. Soc.* **2000**, *122*, 11450.
(27) (a) Castellano, R. K.; Diederich, F.; Meyer, E. A. *Angew. Chem., Int. Ed.* **2001**, *42*, 1211. (b) Brandl, M.; Weiss, M. S.; Jobs, A.; Sühnel, J.; Hilgenfeld, R. *J. Mol. Biol.* **2001**, *307*, 357. (c) Unezawa, Y.; Tsuboyama, S.; Takahashi, H.; Uzawa, J.; Nishio, M. *Bioorg. Med. Chem.* **1999**, *7*, 2021. (d) Fong, T. M.; Cassieri, M. A.; Yu, H; Bansal, A.; Swain, C.; Strader, C. D. *Nature* **1993**, *362*, 350.
(28) (a) Zhao, Y.; Truhlar, D. G. *J. Phys. Chem. A* **2004**, *108*, 6908. (b) Single point calculation at MPWB1K level using the basis sets 6-31+G. (d,p) for H, C, N, O, P and LANL2DZ for Ru on the top of PBE/DNP, DSPP optimised geometries. Calculations performed using Gaussian 03 code . (c) Frisch, M. J.; Trucks, G. W.; Schlegel, H. B.; Scuseria, G. E.; Robb, M. A.; Cheeseman, J. R.; Montgomery, J. A., Jr.; Vreven, T.; Kudin, K. N.; Burant, J. C.; Millam, J. M.; Iyengar, S. S.; Tomasi, J.; Barone, V.; Mennucci, B.; Cossi, M.; Scalmani, G.; Rega, N.; Petersson, G. A.; Nakatsuji, H.; Hada, M.; Ehara, M.; Toyota, K.; Fukuda, R.; Hasegawa, J.; Ishida, M.; Nakajima, T.; Honda, Y.; Kitao, O.; Nakai, H.; Klene, M.; Li, X.; Knox, J. E.; Hratchian, H. P.; Cross, J. B.; Adamo, C.; Jaramillo, J.; Gomperts, R.; Stratmann, R. E.; Yazyev, O.; Austin, A. J.; Cammi, R.; Pomelli, C.; Ochterski, J. W.; Ayala, P. Y.; Morokuma, K.; Voth, G. A.; Salvador, P.; Dannenberg, J. J.; Zakrzewski, V. G.; Dapprich, S.; Daniels, A. D.; Strain, M. C.; Farkas, O.; Malick, D. K.; Rabuck, A. D.; Raghavachari, K.; Foresman, J. B.; Ortiz, J. V.; Cui, Q.; Baboul, A. G.; Clifford, S.; Cioslowski, J.; Stefanov, B. B.; Liu, G.; Liashenko, A.; Piskorz, P.; Komaromi, I.; Martin, R. L.; Fox, D. J.; Keith, T.; Al-Laham, M. A.; Peng, C. Y.; Nanayakkara, A.; Challacombe, M.; Gill, P. M. W.; Johnson, B.; Chen, W.; Wong, M. W.; Gonzalez, C.; Pople, J. A. *Gaussian03*; Gaussian, Inc.: Wallingford, CT, 2004.

Table 2. Energetical and Structural Characterization of the Minima (INT-I, INT-II for Q1 and INT-I for Q2) and Transition-State-like (Hydrog.TS) Structures Associated with the Entrance of the Acetophenone in the Active Sites of *trans*-Ru(H)$_2$(*S*,*S*-dpen)(*S*-xylbinap) along the Q1 and Q2 Pathways As Computed by the DFT-PBE Method[a]

				trans-Ru(H)$_2$(*S*,*S*-dpen)(*S*-xylbinap)					acetophenone			
		ΔE	r(CH$_1$)	r(RuH$_1$)	r(RuH$_2$)	r(RuN)	r(RuP)	r(N−H)	r(CO)	r(OH)	τ	γ
Q1	INT-I	−13.23	3.76	1.72	1.71	2.20	2.25	1.02	1.23	3.42	1.0	−4.5
	INT-II	−23.01	3.65	1.72	1.70	2.21	2.25	1.02	1.23	3.79	1.1	19.8
	TS	−7.61	2.00	1.78	1.67	2.18	2.27	1.04	1.26	1.95	16.2	20.4
Q2	INT-I	−17.50	3.77	1.72	1.70	2.20	2.25	1.02	1.24	3.52	1.5	−4.0
	TS	9.58	1.90	1.82	1.66	2.19	2.27	1.04	1.26	1.93	20.4	−41.3

[a] Energies in kilojoules per mole, distances in angstroms, and angles in degrees. ΔE electronic energy difference with respect to energy at 9 Å separation; τ out-of-plane bending of the carbonyl carbon; γ torsional angle of the phenyl group along the C−C(=O) bond.

from 2.36 Å in INT-I to 2.48 Å in INT-II (the sum of the van der Waals H···H radii is 2.4 Å).

The energies of the intermediates INT-I, INT-II and of the separated reactants (taken at 9 Å) have also been evaluated at the MPWB1K level.[28] As discussed previously, the stabilization of the intermediates is based on noncovalent XH/π interactions. An assessment of 44 DFT methods and 1 wave function theory method (MP2) against a benchmark database of Binding Energies (BEs) for nonbonded interaction complexes (which consisted of hydrogen bonding, charge transfer, dipole interactions and weak dispersionlike interactions) showed that MPWB1K is one of the best tested density functionals for these interactions and that it also outperforms the MP2 method.[29] Furthermore, this study showed that PBE (the density functional used in the present work to compute structures and total energies) was also accurate in the evaluation of hydrogen bonding and weak interaction complexes and that it performs considerably better than the popular B3LYP functional. Similar conclusions are reported in a very recent study.[30] The computed MPWB1K extra-stabilization energy of INT-II with respect to INT-I is 11.13 kJ/mol, in good agreement with the value obtained using the PBE functional (9.78 kJ/mol). This result further justifies the use in the present study of the computationally convenient PBE functional.

The intermediates INT-I and INT-II along the Q1 approach correspond therefore to two (local) minima for the system [*trans*-Ru(H)$_2$(*S*,*S*-dpen)(*S*-xylbinap) + acetophenone]. It is important to notice that the "spike" along the H-transfer reaction coordinate at 2.7 Å (see Figure 3) does not correspond to the transition state structure for the conformational change between INT-I and INT-II. In fact, in Figures 2 and 3 we are probing the PES along (Ru−)H···C(=O) while INT-I and INT-II are actually characterized by (Ru−)H···C(=O) ∼ 3.7 Å [in Table 2, r(CH$_1$) = 3.76 Å in INT-I and r(CH$_1$) = 3.65 Å in INT-II]. To demonstrate the existence of a continuous and energetically accessible pathway which connects the species INT-II and INT-I, we have considered a conformational interconversion where, starting from INT-II, the first step is the rotation of the phenyl group from +20° to ∼−5°, followed by the rotation of the acetophenone molecule with respect to an axis which belongs to the plane defined by C−C=O, passes through the carbonyl C and is perpendicular to the C=O bond, allowing the acetophenone to leave the chiral pocket. Note that INT-II is characterized by r(CH$_1$) = 3.65 Å, r(OH) = 3.79 Å and γ = +19.8° [γ is the torsional angle of the phenyl group along the C−C(=O) bond], while INT-II is characterized by r(CH$_1$) = 3.76 Å, r(OH) = 3.42 Å and γ = −4.5° (see Table 2). To calculate the interconversion pathway described above we have considered the following procedure: (i) Starting from INT-II the PES of [*trans*-Ru(H)$_2$(*S*,*S*-dpen)(*S*-xylbinap) + acetophenone] has been scanned with respect to γ, with −25° < γ < +20° [see Figure 6a]. (ii) From point (2) in Figure 6a, which is characterized by γ = −10,° r(CH$_1$) = 3.77 Å [these values for r(CH$_1$) and γ are the closest to the ones we have in INT-I] and r(OH) = 4.19 Å, we have calculated the PES of [*trans*-Ru(H)$_2$(*S*,*S*-dpen)(*S*-xylbinap) + acetophenone] with respect to r(OH), with 4.1 Å < r(OH) < 3.4 Å, at the fixed values of γ = −10° and r(CH$_1$) = 3.77 Å [see Figure 6b]. The energy profiles associated with this conformational change in Figure 6 demonstrate the existence of a continuous and energetically accessible interconversion pathway from (1) ≡ INT-II to (2), and from (2) to (3) ≈ INT-I. Furthermore, starting from point (3) in Figure 6b, the constraints applied to r(OH), r(CH$_1$), and γ have been removed and the structure freely optimized. In the resulting structure the acetophenone is outside the chiral pocket, its geometry is characterized by r(CH$_1$) = 3.69 Å, r(OH) = 3.42 Å and γ = −6.8°, very close to INT-I, and its relative energy differs by less than 2 kJ/mol with respect to INT-I.

For the Q1 approach, we finally consider the structure of Hydrog.TS (see Figure 4 and Table 2). In particular, we note that the torsional angle of the phenyl group in Hydrog.TS (γ = 20.4°) is the same as in the intermediate INT-II (γ = 19.8°). This corroborates the hypothesis that, along the Q1 pathway, there is a recognition step, the formation of the stable intermediate INT-II, determined by the rearrangement of the phenyl group [rotation along the C−C(=O)] in order to have a conformation for the acetophenone closer to that in the transition state structure. With regard to the other Hydrog.TS structural parameters, the lengthening of the Ru−H$_1$, N−H, C=O bonds, the shortening of the Ru−H$_2$, Ru−N, Ru−P bonds, and the change of the carbonyl C hybridization (in Table 2, τ changes from 1.1° in INT-II to 16.2° in Hydrog.TS) indicate forming and breaking of bonds at the transition state level. Note that we have verified that Hydrog.TS and INT-II are connected by relaxing the structure of Hydrog.TS after giving a small perturbation in order to

(29) Zhao, Y.; Truhlar, D. G. *J. Chem. Theory Comput.* **2005**, *1*, 415.
(30) Zhao, Y.; Truhlar, D. G. *J. Chem. Theory Comput.* **2007**, *3*, 289.
(31) Calculations performed at PBE/DNP level of theory for the hydrogen transfer acetone/*i*-propyl alcohol reaction catalysed by model *trans*-Ru(H)$_2$(diphosphine)(diamine) catalysts. The structure of the optimized transition states can be found in Table 5.

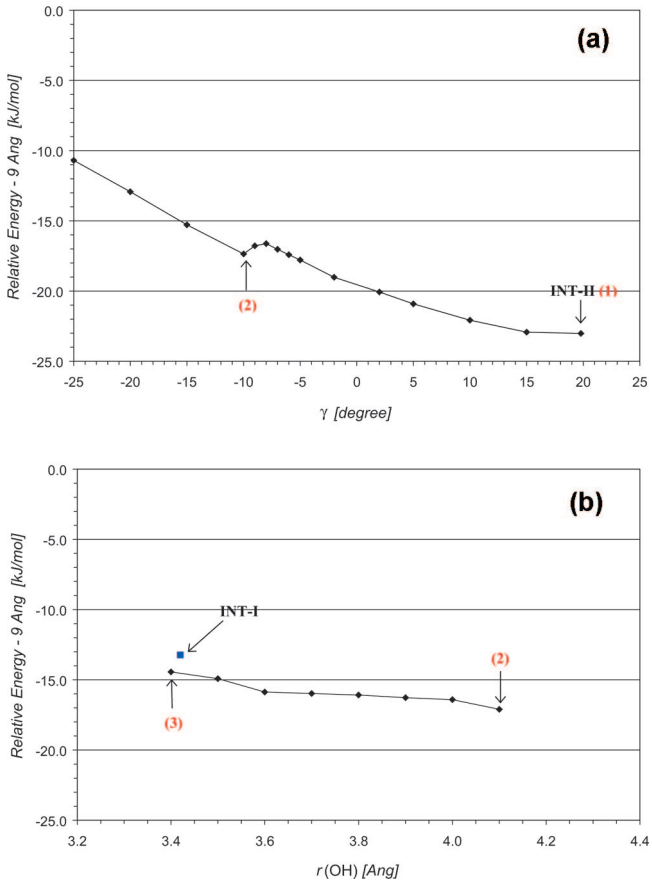

Figure 6. Potential energy curve of the [*trans*-Ru(H)$_2$(*S*,*S*-dpen)(*S*-xylbinap) + acetophenone] with respect to torsional angle of the phenyl group γ (a) and with respect to the *r*(OH) internuclear distance (b) for the Q1 approach. Values computed at the DFT-PBE level of theory.

obtain the reactant. From Table 2, the computed internuclear distances of the Hydrog.TS structure agree with previous studies on hydrogen transfer ketone/alcohol reactions catalyzed by model Ru(H)$_2$(diphosphine) (diamine) catalysts.[19–31] Moreover, the computed activation energy for the H-transfer acetophenone/(*R*)-phenylethanol reaction (15.40 kJ/mol) is quite close to the reaction barrier for the hydrogen transfer acetone/*i*-propyl alcohol reaction catalyzed by model Ru(H)$_2$(diphosphine)(diamine) catalysts (9.01 kJ/mol).[19–31]

For the Q2 approach, the minimum INT-I is analogous to the intermediate INT-I along Q1. In fact, the intermediate INT-I in Figure 5 corresponds to the situation where the acetophenone is outside the pocket; the phenyl group of the acetophenone is approximately on the plane defined by the C−C═O nuclei (in Table 2, $\gamma = -4.0°$ for INT-I of Q2) and the carbonyl carbon displays sp2 character (in Table 2, $\tau = 1.5°$). No other intermediate has been located along the Q2 pathway and in the Hydrog.TS structure the conformational structure of the acetophenone is very different from the conformation in INT-I (see Figure 5). In particular, the torsional angle γ changes drastically from −4.0 ° in INT-I to −41.3 ° in Hydrog.TS (see Table 2).

Why must the phenyl group be rotated by so much in the Hydrog.TS structure associated with the Q2 approach? Starting from INT-I, as the acetophenone approaches the *trans*-Ru(H)$_2$(*S*,*S*-dpen)(*S*-xylbinap) catalyst, the steric interaction between the phenyl group of the acetophenone and the methyl groups in meta position increases, and so does the energy of the system (see Figure 3). In Figure 7, the structure of a hypothetical transition state for the Q2 approach is reported, which has been obtained by taking the Hydrog.TS structure in Figure 5 and fixing the torsional angle γ to −4.0° (the torsional angle of the phenyl group in INT-I, see Table 2). Because of the close H···H contacts (see Figure 7) the energy of this hypothetical transition state drastically increases by 48 kJ/mol with respect to Hydrog.TS in Figure 5. This corroborates the hypothesis that along Q2, the large rotation of the phenyl group from −4.0 ° in INT-I to −41.3 ° in Hydrog.TS is connected to the increased steric interaction between the phenyl group of the acetophenone and the methyl groups in the meta position. Therefore, when the reaction proceeds along the Q2 pathway, there is an extra energy cost associated with the torsion of the phenyl group on transforming the reactant-complex INT-I to the Hydrog.TS. We have estimated this extra energy cost by computing the PES of acetophenone with respect to the internal rotation of the phenyl group, scanning the torsional angle from 0° to 360° (see Figure 8). At the PBE level, the energy difference between the conformation of the acetophenone with $\gamma = 4.0°$ and the conformation with $\gamma = 40°$ is

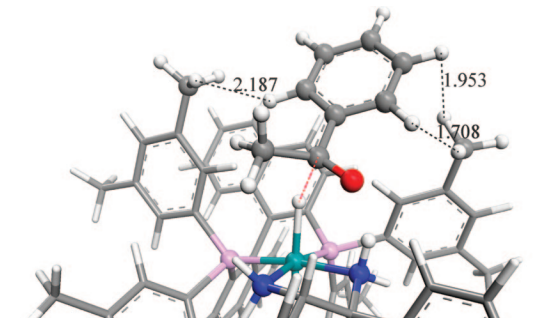

Figure 7. Hypothetical transition state structure for the [*trans*-Ru(H)$_2$(*S*,*S*-dpen)(*S*-xylbinap) + acetophenone] system along the Q2 pathway obtained from Hydrog.TS reported in Figure 5 by fixing the torsional angle $\gamma = -4.0°$.

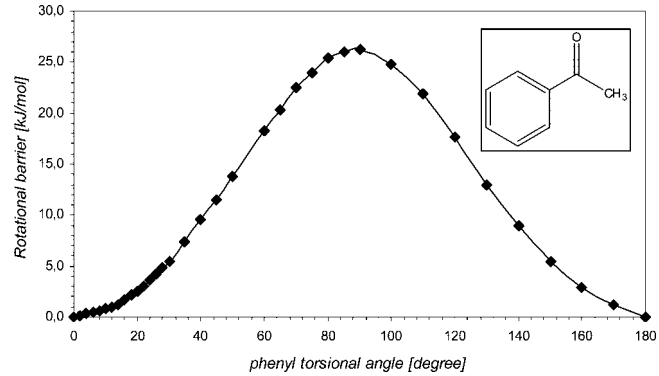

Figure 8. Potential energy curve of the acetophenone for internal rotation of the phenyl group about the C−C bond. Values computed at the DFT-PBE level of theory.

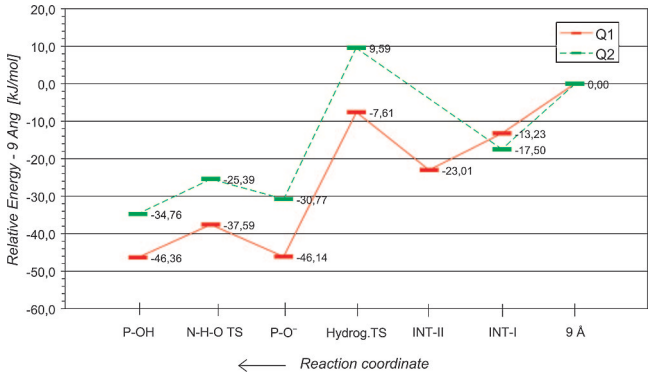

Figure 9. Potential energy surface for the hydrogen transfer acetophenone−phenylethanol reaction catalysed by the *trans*-Ru(H)$_2$(*S*,*S*-dpen)(*S*-xylbinap) as computed by the DFT-PBE method.

approximately 9 kJ/mol. The difference between the activation energy for the reduction of acetophenone to (*R*)-phenylethanol (ΔE^{a}_{Q1} = 15.40 kJ/mol) and the activation energy for the reduction of acetophenone to (*S*)-phenylethanol (ΔE^{a}_{Q2} = 27.08 kJ/mol) is 11.68 kJ/mol, which is close to 9 kJ/mol. Therefore, when the acetophenone approaches the catalyst **1** along the Q1 reaction pathway, the activation energy is associated only with the H-transfer process: $\Delta E^{a}_{Q1} \cong \Delta E_{\text{H-transfer}}$. On the other hand, for the Q2 approach the activation energy can be considered as given by the sum of the H-transfer and phenyl rotation processes: $\Delta E^{a}_{Q2} \cong \Delta E_{\text{H-transfer}} + \Delta E_{\text{ph-rotation}}$. It has been previously observed that the H···H interaction between the methyl group of the acetophenone and the methyl group of the phosphorus aryl substituent in meta position is decreased in going from INT-I to INT-II.

Therefore, the analysis of the intermediates and transition state structures for the *trans*-Ru(H)$_2$(*S*,*S*-dpen)(*S*-xylbinap)-catalyzed acetophenone hydrogenation along the competitive Q1 [(*R*)-phenylethanol] and Q2 [(*S*)-phenylethanol] pathways shows that the high enantioselectivity for the *R*-alcohol can be explained in terms of the existence of a stable intermediate (INT-II) along the Q1 reaction pathway, where the acetophenone has the same conformation as in the in the Hydrog.TS structure. The formation of this intermediate is hindered for the competing pathways. For the Q2 approach, we have demonstrated that the absence of an intermediate like INT-II increases the activation energy because of the extra energy cost associated with the rotation of the phenyl group on going from INT-I to Hydrog.TS.

Further analysis and insights is gained from the PES given in Figure 9 for the hydrogen transfer acetophenone-phenylethanol reaction catalyzed by *trans*-Ru(H)$_2$(*S*,*S*-dpen)(*S*-xylbinap) as computed by the DFT-PBE method. First, we observe that *trans*-Ru(H)$_2$(*S*,*S*-dpen)(*S*-xylbinap) effectively discriminates between the two prochiral faces of the acetophenone. Indeed, both the binding energies ($BE_{Q1} > BE_{Q2}$) and the activation energies ($\Delta E^{a}_{Q1} < \Delta E^{a}_{Q2}$) determine that Q1 is the most favorable reaction pathway. Therefore, the preference for the (*R*)-alcohol is driven both by thermodynamic and kinetic factors.

To gain further information on the mechanism, we started from the two diastereomeric Q1 and Q2 Hydrog.TS; the

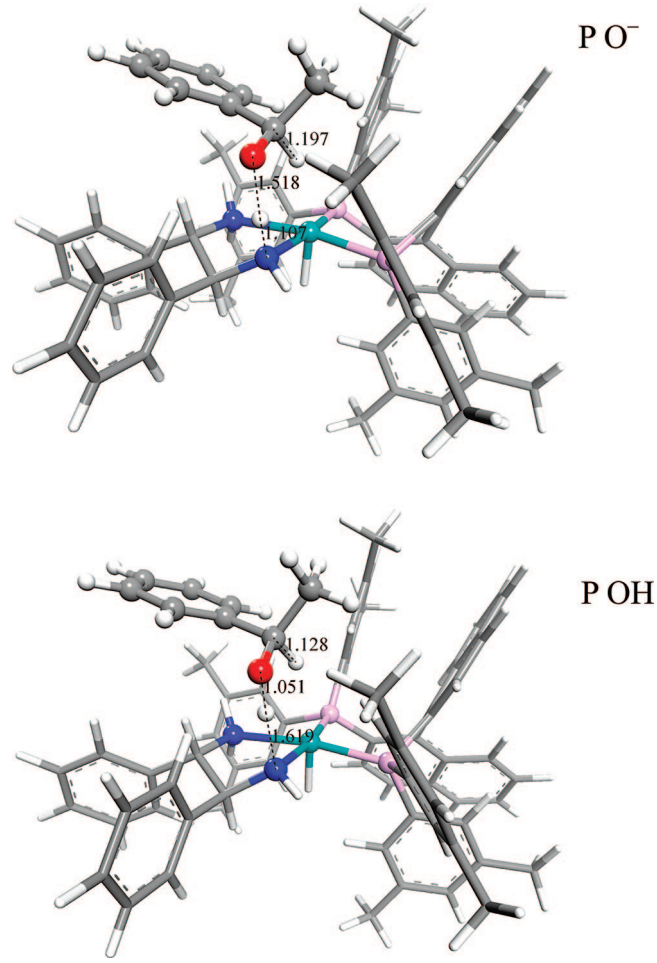

Figure 10. Structures of the product complex intermediates P−O$^-$ and P−OH associated with the *trans*-Ru(H)$_2$(*S*,*S*-dpen)(*S*-xylbinap)-catalyzed acetophenone reduction along the Q1 approach as computed by the DFT-PBE method.

transition state structures were relaxed after giving a small perturbation in order to obtain the alcohol products. In both cases, the resulting optimized structure (P−O$^-$ in Figure 9) corresponds to the situation where only the (Ru−)H hydride is transferred to the carbonyl carbon (for the Q1 approach, see Figure 10), but the (N−)H protic is still bound to the nitrogen atom and interacts with the O atom through a hydrogen bond. Starting from the intermediate P−O$^-$, the PES of the system has been scanned with respect to the N−H and O−H internuclear distances, which were simultaneously kept at fixed values at each stage of the geometry optimization. The maxima along the resulting energy profile was used to approximate the energy barrier between the intermediates P−O$^-$ and P−OH (see Figure 9), where the hydrogen is actually bound to the oxygen. In Figure 10, the structures of P−O$^-$ and P−OH correspond to the switch from the situation where the N−H is the donor and O is the acceptor (P−O$^-$) to the situation where O−H is the donor and N is the acceptor of a hydrogen bond-like interaction. In fact, for P−O$^-$ the length of N−H (1.11 Å) in N−H···O correlates very well with the H···O distance (1.52 Å) observed experimentally

(32) Correlation based on low temperature neutron diffraction data. Steiner, T.; Majerz, I.; Wilson, C. C. *Angew. Chem., Int. Ed.* **2001**, *40*, 2651.

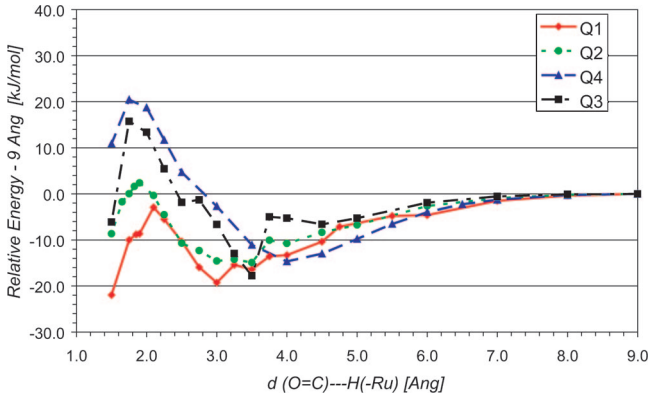

Figure 11. Electronic energy variation of the system [*trans*-Ru(H)$_2$(*S*,*S*-dpen)(*S*-tolbinap) + acetophenone] along the [(Ru−)H···C(=O)] internuclear distance for each possible approach (Q1, Q2, Q3, Q4). Values computed at the DFT-PBE level of theory.

(1.50 Å).[32] In the same way, for P−OH, the length of O−H (1.05 Å) correlates quite well with the H···N distance (1.62 Å) measured experimentally (1.55 Å).[32] Our calculations suggest therefore that in gas-phase the H-transfer ketone/alcohol reaction catalyzed by Ru(diphosphine)(diamine) is a stepwise mechanism: first the Ru coordinated hydride is transferred to the carbonyl carbon (INT-II → Hydrog.TS → P−O$^-$) and only in a subsequent step of the reaction mechanism is the amine proton donated to the oxygen atom (P−O$^-$ → N−H−O TS → P−OH). This result differs from the mechanism postulated by Noyori and co-workers, where the hydride Ru−H and protic N−H are simultaneously transferred to the C=O functionality. The result obtained here for the reduction of acetophenone promoted by *trans*-Ru(H)$_2$(*S*,*S*-dpen)(*S*-xylbinap), has been confirmed by calculations on the [acetophenone + *trans*-Ru(H)$_2$(*S*,*S*-dpen)(*S*-tolbinap)] and [cyclohexyl methyl ketone + *trans*-Ru(H)$_2$(*S*,*S*-dpen)(*S*-xylbinap)] systems (vide infra). However, it is important to note that the barrier for this H-transfer is very low (∼2 kcal/mol) and hydrogen atom tunnelling through the barrier is certainly playing a role, as H is a light element and the distance that the atom has to cover is short (∼0.3–0.4 Å). Moreover, gas-phase calculations of the type reported here cannot deny the solvent incorporated mechanisms as reported by Maijer, where the methanol molecules played an active role in the ruthenium-catalyzed transfer hydrogenation reaction converting formaldehyde into methanol.[5] However, the main aim of the present study is the elucidation of the factors controlling enantioselectivity in Ru(diphosphine)(diamine) hydrogenation catalysts rather than focusing on details of the mechanism such as the effect of the solvent molecules in the H-transfer step, which is unlikely to affect the enantioselectivity. In fact, it has been demonstrated here that the differentiation of two prochiral faces in the case of the acetophenone molecule resides in the "docking" of the substrate into the reactive pocket (formation of INT-II) well before the breaking/forming interactions at the transition state level are established.

3.2. Reduction of Acetophenone by *trans*-Ru(H)$_2$(*S*,*S*-dpen)(*S*-tolbinap). Figure 11 shows the variation in energy of the system [**2** + acetophenone] as a function of the pseudo reaction coordinate (Ru−)H···C(=O) for each possible approach of the acetophenone to the active sites of the catalysts (Q1, Q2, Q3 and Q4). The maximum energy centered at approximately 2 Å along the reaction coordinate corresponds to the transition state structure for the hydrogen transfer acetophenone−phenylethanol reaction (Hydrog.TS). The energies of the Hydrog.TS relative to that of the separated reactants (considered at 9 Å) are: −2.91 kJ/mol for Q1, 2.39 kJ/mol for Q2, 15.74 kJ for Q3 mol^{-1}, and 20.48 kJ/mol for Q4.

For the Q1 approach in particular, the electronic energy chart of the [**2** + acetophenone] system displays a very different profile from [**1** + acetophenone]. Indeed, the Q1 pathway for [**2** + acetophenone] does not display any double energy well (see Figures 3 and 4) and therefore the PES of [**2** + acetophenone] along the Q1 approach is characterized by a single reactant−complex intermediate.

The minima at approximately 3 Å along Q1 and Q2 have been freely optimized. The energetics and optimized stuctures of the intermediate (INT-I) and the transition state (Hydrog.TS) associated with the most competitive approaches (Q1 and Q2) are summarized in Table 3 and illustrated in Figure 12.

From the results reported in Table 3, the BE of acetophenone to the active site of the catalyst **2** along Q1 (−19.45 kJ/mol) is larger than the BE along Q2 (−14.74 kJ/mol). In contrast, the activation energy for the hydrogen transfer acetophenone/phenylethanol reaction along Q1 (16.54 kJ/mol) is very close to the reaction barrier along Q2 (17.13 kJ/mol). Therefore, our DFT-PBE calculations suggest that the preference for the (*R*)-phenylethanol in the *trans*-Ru(H)$_2$(*S*,*S*-dpen)(*S*-tolbinap)-catalyzed acetophenone hydrogenation is only driven by the binding process ($BE_{Q1} > BE_{Q2}$) and not by kinetic factors ($\Delta E^a_{Q1} \approx \Delta E^a_{Q2}$). This result qualitatively explains the lower enantioselectivity observed for the reduction of acetophenone catalyzed by *trans*-Ru(H)$_2$(*S*,*S*-dpen)(*S*-tolbinap) compared with the *trans*-Ru(H)$_2$(*S*,*S*-dpen)(*S*-xylbinap)-catalyzed reaction (see Scheme 1).

With regards to the structural parameters reported in Table 3, the out-of-plane angle τ suggests that the carbonyl carbon in the intermediates INT-I has sp^2 character ($\tau = 0.23°$ for Q1 and $\tau = 0°$ for Q2), while the lengthening of the Ru−H$_1$, N−H, C=O bonds, the shortening of the Ru−H$_2$, Ru−N, Ru−P bonds, and the change of C hybridization ($\tau = 0.23°$ in INT-I to 13.6° in Hydrog.TS for Q1, $\tau = 0°$ in INT-I to 17.6° in Hydrog.TS for Q2) indicate forming and breaking of bonds at the transition state level. Furthermore, the acetophenone conformation in INT-I is close to the conformation in the Hydrog.TS structure ($\gamma = 12.5°$ in INT-I to 11.5° in Hydrog.TS for Q1; $\gamma = -8.0°$ in INT-I to −0.1° in Hydrog.TS for Q2). This is a substantial difference from what is observed for [**1** + acetophenone], where the conformation of the acetophenone in the intermediate INT-I is very different from the conformation in the Hydrog.TS structure, and the formation of a second intermediate along Q1 (INT-II) represents the recognition step for the stereodifferentiation of Q1 and Q2.

Table 3. Energetic and Structural Characterization of the Minima (INT-I) and Transition-State-like (Hydrog.TS) Structures Associated with the Entrance of the Acetophenone in the Active Sites of *trans*-Ru(H)$_2$(*S*,*S*-dpen)(*S*-tolbinap) along the Q1 and Q2 Pathways As Computed by the DFT-PBE Method[a]

				trans-Ru(H)$_2$(*S*,*S*-dpen)(*S*-tolbinap)					acetophenone			
		ΔE	r(CH$_1$)	r(RuH$_1$)	r(RuH$_2$)	r(RuN)	r(RuP)	r(N−H)	r(CO)	r(OH)	τ	γ
Q1	INT-I	−19.45	3.13	1.72	1.71	2.21	2.25	1.02	1.23	2.77	0.2	12.5
	TS	−2.91	2.10	1.78	1.67	2.19	2.26	1.03	1.25	1.98	13.6	11.5
Q2	INT-I	−14.74	3.10	1.71	1.71	2.22	2.25	1.02	1.23	2.87	0.0	−8.0
	TS	2.39	1.90	1.82	1.66	2.18	2.26	1.04	1.26	1.92	17.6	−0.1

[a] Energies in kilojoules per mole, distances in angstroms, and angles in degrees. ΔE electronic energy difference with respect to energy at 9 Å separation; τ out-of-plane bending of the carbonyl carbon; γ torsional angle of the phenyl group along the C−C(=O) bond.

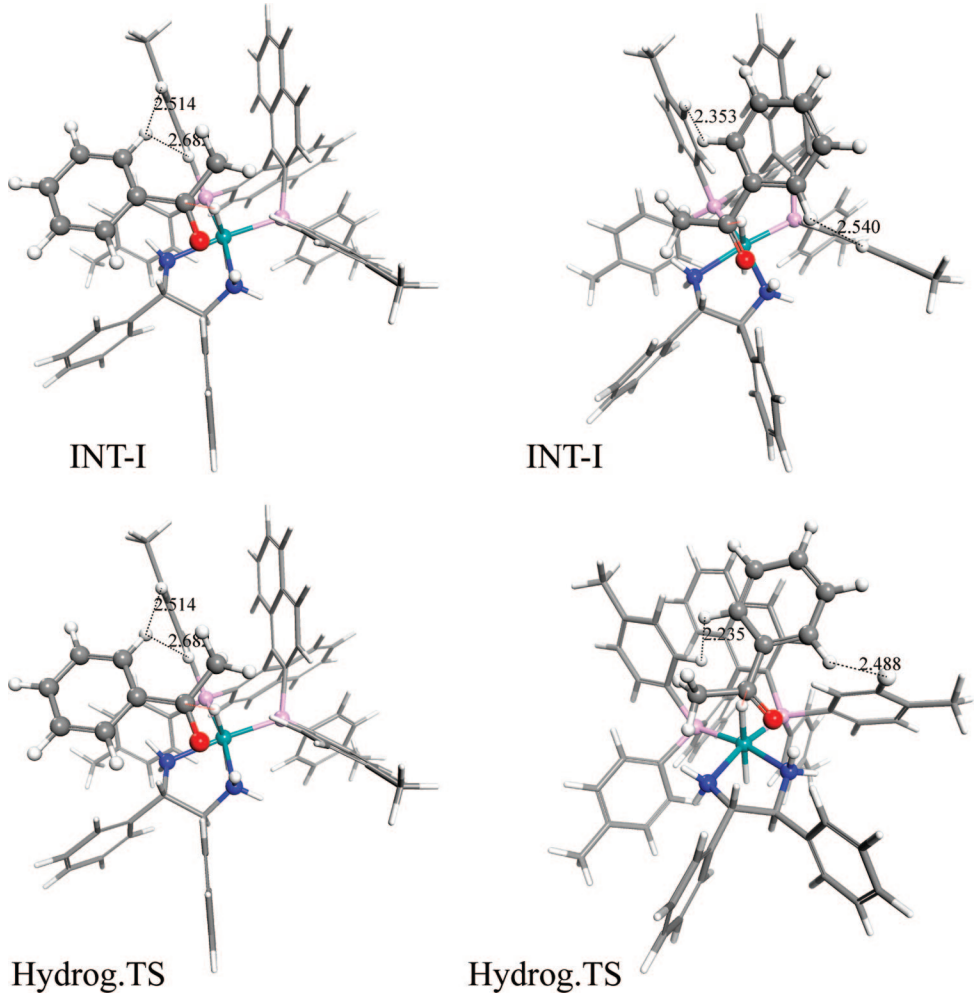

Figure 12. Minima (INT-I) and transition-state (Hydrog.TS) structures for acetophenone entry in the active sites of the *trans*-Ru(H)$_2$(*S*,*S*-dpen)(*S*-tolbinap) catalyst along the Q1 and Q2 pathways as computed by the DFT-PBE method.

Figure 13 shows the PES for the hydrogen transfer acetophenone-phenylethanol reaction catalyzed by *trans*-Ru(H)$_2$(*S*,*S*-dpen)(*S*-tolbinap). For Q1 and Q2, the reduction of acetophenone proceeds through a single step, which corresponds to the H-transfer process, and there is no stereodetermining process associated with the conformational change of the ketone to differentiate the two prochiral faces of the ketone. The activation energies for the reduction of acetophenone by **2** along Q1 and Q2 are therefore very similar because, in both approches, the H-transfer is the only process involved. This result also explains why the activation energy of [**1** + acetophenone] along Q1 (15.40 kJ/mol) is close to the activation energy for [**2** + acetophenone] along Q1 (16.54 kJ/mol) and Q2 (17.13 kJ/mol), and corroborates our hypothesis that, for the class of catalysts in Scheme 1, the enantioselectivity of the reaction should not only depend in changes at transition state level, but should reside in the docking of the ketone into the reactive pocket well before the bond breaking/forming interactions are established.

Figure 12 shows the optimized structures of the intermediates INT-I along Q1 and Q2. For Q2, the phenyl group of the acetophenone lies in between the phosphorus atoms of the diphosphine ligand and the steric interaction with the bulky aryl groups of the diphosphine is larger than in the Q1 intermediate. In fact, the minimum H···H distances reported in Figure 12 indicate that on going from Q2 to Q1, the steric interaction decreases, explaining the larger BE associated with the Q1 approach (see Table 3). The analysis

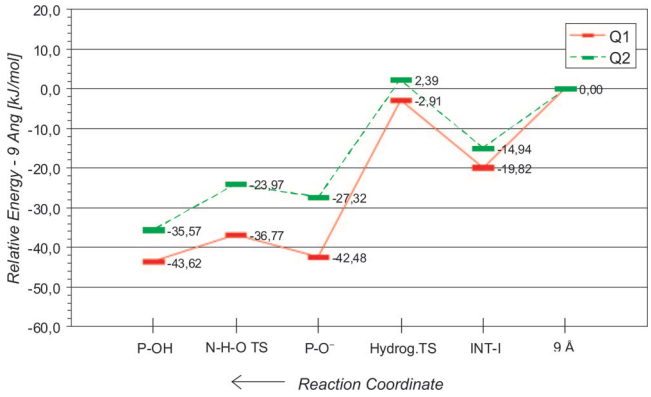

Figure 13. Potential energy surface for the hydrogenation of acetophenone catalysed by the *trans*-Ru(H)$_2$(*S*,*S*-dpen)(*S*-tolbinap) as computed by the DFT-PBE method.

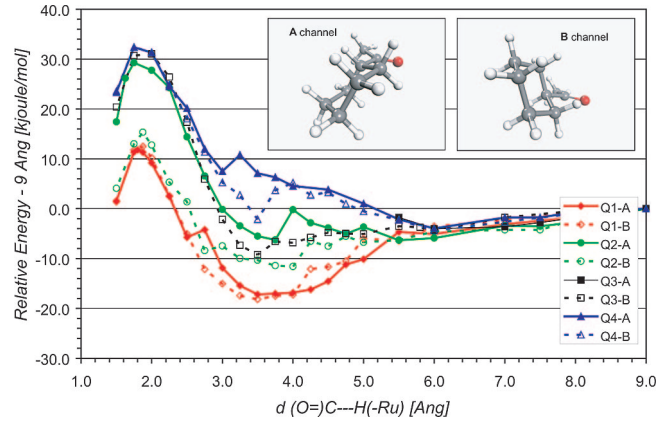

Figure 14. Electronic energy variation of the system [*trans*-Ru(H)$_2$(*S*,*S*-dpen)(*S*-xylbinap) + cyclohexyl methyl ketone] along the [(Ru−)H···C(=O)] internuclear distance for each possible approach (Q1, Q2, Q3, Q4). Values computed at the DFT-PBE level of theory.

of the Hydrog.TS structures shows that for the Q2 approach the minimum H···H distances between the phenyl group of the acetophenone and the (4-methyl)-phenyl substituents of the phosphorus atoms are 2.235 Å and 2.187 Å (compared to 2.187 Å and 1.708 Å in the hypothetical transition state structure of [**1** + acetophenone] reported in Figure 7). Therefore, in the case of the acetophenone approach on the active sites of *trans*-Ru(H)$_2$(*S*,*S*-dpen)(*S*-tolbinap) along the Q2 pathway, the lack of methyl groups in the meta position does not induce the drastic rotation of the phenyl group along the C−C(=O) bond ($\gamma = -8.0°$ in INT-I to $\gamma = -0.1°$ in Hydrog.TS) observed for the [**1** + acetophenone] system ($\gamma = -4.0°$ in INT-I to $\gamma = -41.3$ ° in Hydrog.TS).

Finally, as previously observed for the [**1** + acetophenone] system, the reaction profile computed for [**2** + acetophenone] (see Figure 13) indicates that in gas-phase the mechanism for the H-transfer reaction is a stepwise mechanism: in the first step, the (Ru−)H hydride is transferred to the carbonyl C and in the second the protic (N−)H is donated to the O.

3.3. Reduction of Cyclohexyl Methyl Ketone by *trans*-Ru(H)$_2$(*S*,*S*-dpen)(*S*-xylbinap). For the cyclohexyl methyl ketone, an analysis of the potential barrier for internal rotation of the cyclohexyl group about the C−C(=O) has shown that there are two conformational isomers (see Figure 14), with the conformer **B** 0.39 kJ/mol lower in energy than **A**. Consequently, for each possible approach (Q1, Q2, Q3, and Q4) of the dialkyl ketone to the active sites of *trans*-Ru(H)$_2$(*S*,*S*-dpen)(*S*-xylbinap) there are two possible "channels" (**A** and **B**), which correspond to the two conformers of the cyclohexyl methyl ketone. Therefore, to study the enantioselectivity for the reaction reported in Scheme 2, we had to compute a total of eight energy profiles along the (Ru−)H···C(=O) reaction coordinate.

In Figure 14, the energy variation of the system [**1** + cyclohexyl methyl ketone] as a function of the pseudo reaction coordinate (Ru−)H···C(=O) for each possible approach of the dialkylketone (Q1-**A**, Q1-**B**,Q2-**A**, Q2-**B**, Q3-**A**, Q3-**B**, Q4-**A**, and Q4-**B**) is displayed. The energy profile associated with Q3-**A** is incomplete because the geometry optimization did not converge when the constraint applied to (Ru−)H···C(=O) was ≤5.5 Å. The maximum energy centered at approximately 1.9 Å along the reaction coordinate corresponds to the Hydrog.TS for the H-transfer cyclohexyl

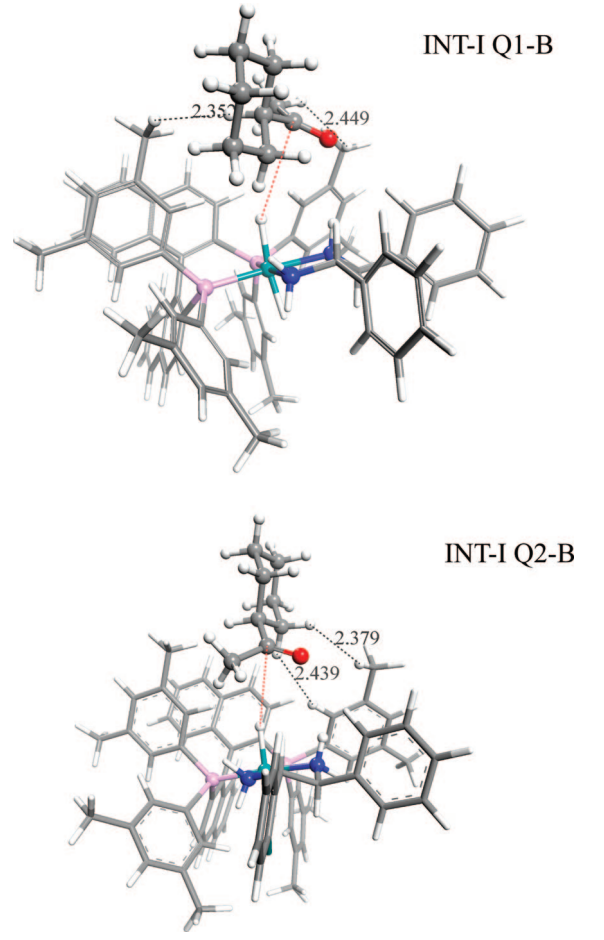

Figure 15. Minima (INT-I) structures for cyclohexyl methyl ketone entry in the active sites of the *trans*-Ru(H)$_2$(*S*,*S*-dpen)(*S*-xylbinap) catalyst along the Q1-B and Q2-B pathways as computed by the DFT-PBE method.

methyl−cyclohexyl methyl alcohol reaction. Note that all Hydrog.TS structures are higher in energy than the separated reactants (considered at 9 Å). For the Q1 approach, this contrasts sharply with the system [**1** + acetophenone], whose Hydrog.TS is −7.91 kJ/mol more stable than the separated reactants [see Table 2].

No minima have been located along the reaction profiles Q4-**A** and Q4-**B**, while the minima at approximately 3.5–4

Table 4. Energetic and Structural Characterization of the Minima (INT-I) and Transition-State-like (Hydrog.TS) Structures Associated with the Entrance of the Cyclohexyl Methyl Ketone in the Active Sites of *trans*-Ru(H)$_2$(*S*,*S*-dpen)(*S*-xylbinap) along the Q1 and Q2 Pathways As Computed by the DFT-PBE Method[a]

				trans-Ru(H)$_2$(*S*,*S*-dpen)(*S*-xylbinap)					cyclohexyl methyl ketone		
		ΔE	r(CH$_1$)	r(RuH$_1$)	r(RuH$_2$)	r(RuN)	r(RuP)	r(N−H)	r(CO)	r(OH)	τ
Q1-**A**	INT-I	−19.51	3.55	1.72	1.71	2.21	2.25	1.02	1.23	3.38	0.4
	TS	10.98	1.80	1.84	1.65	2.18	2.27	1.04	1.27	1.86	22.0
Q1-**B**	INT-I	−17.92	3.45	1.72	1.71	2.20	2.25	1.02	1.23	3.15	0.4
	TS	12.50	1.88	1.82	1.66	2.19	2.27	1.04	1.28	1.93	20.0
Q2-**A**	INT-I	−11.35	4.16	1.71	1.71	2.20	2.25	1.02	1.23	3.48	0.4
	TS	29.28	1.75	1.88	1.64	2.17	2.28	1.05	1.27	1.74	24.7
Q2-**B**	INT-I	−17.86	3.52	1.72	1.71	2.21	2.25	1.02	1.23	3.27	0.2
	TS	15.33	1.88	1.82	1.66	2.18	2.28	1.04	1.26	1.94	19.4
Q3-**B**	INT-I	−17.05	4.13	1.72	1.70	2.21	2.25	1.02	1.23	4.28	0.4
	TS	30.73	1.75	1.84	1.65	2.19	2.26	1.05	1.27	1.77	20.8

[a] Energies in kilojoules per mole, distances in angstroms, and angles in degrees. ΔE electronic energy difference with respect to energy at 9 Å separation; τ out-of-plane bending of the carbonyl carbon; γ torsional angle of the phenyl group along the C−C(=O) bond.

Table 5. Structure (in angstroms) of the Optimized Transition States of the Hydrogen Transfer Acetone/*i*-Propyl Alcohol Catalyzed by Model *trans*-Ru(H)$_2$(diphosphine)(diamine) Catalysts As Computed by the DFT-PBE Method

	1[a]	**2**[b]	**3**[c]	**4**[d]	**5**[e]	**6**[f]	**7**[g]	**8**[h]	approximated Hydrog.TS[i]
r(Ru−N)	2.204	2.198	2.190	2.195	2.218	2.204	2.208	2.208	2.184
r (Ru−P)	2.228	2.237	2.225	2.227	2.229	2.232	2.238	2.238	2.271
r(Ru−H)	1.749	1.750	1.748	1.746	1.747	1.752	1.748	1.751	1.833
r (N−H)	1.037	1.038	1.036	1.037	1.036	1.039	1.037	1.038	1.041
r (C−H)	1.953	1.919	1.940	1.939	1.949	1.872	1.873	1.896	1.800
r (O−H)	1.859	1.841	1.860	1.858	1.871	1.820	1.859	1.828	1.867
r(C=O)	1.251	1.253	1.252	1.251	1.251	1.254	1.254	1.253	1.266

[a] **1**: Ru(H)$_2$(PH$_2$CHCHCHCHPH$_2$)(NH$_2$CH$_2$CH$_2$NH$_2$). [b] **2**: Ru(H)$_2$[PH$_2$CHC(CHMe$_2$)C(CHMe$_2$)CHPH$_2$](NH$_2$CH$_2$CH$_2$NH$_2$). [c] **3**: Ru(H)$_2$[PH$_2$CHCHCHCHPH-(CH$_3$)](NH$_2$CH$_2$CH$_2$NH$_2$). [d] **4**: Ru(H)$_2$[PH$_2$CHCHCHCHP(CH$_3$)$_2$](NH$_2$CH$_2$CH$_2$NH$_2$). [e] **5**: Ru(H)$_2$[PH(CH$_3$)CHCHCHCHP(CH$_3$)$_2$](NH$_2$CH$_2$CH$_2$NH$_2$). [f] **6**: Ru(H)$_2$[PH$_2$CHCHCHCHPH(Ph)](NH$_2$CH$_2$CH$_2$NH$_2$), where Ph is a phenyl group. [g] **7**: Ru(H)$_2$[PH(Ph)CHCHCHCHPH(Ph)](NH$_2$CH$_2$CH$_2$NH$_2$), where Ph is a phenyl group. [h] **8**: Ru(H)$_2$[PH(Ph)CHCHCHCHP(Ph)$_2$](NH$_2$CH$_2$CH$_2$NH$_2$), where Ph is a phenyl group. [i] Approximated Hydrog.TS: transition state of the hydrogen transfer cyclohexyl methyl ketone/cyclohexyl methyl alcohol reaction catalysed by *trans*-Ru(H)$_2$(*S*,*S*-dpen)(*S*-xylbinap) catalyst (**1**) as computed by the DFT-PBE method obtained as the maximum point along the pseudo reaction coordinate (Ru−)H···C(=O).

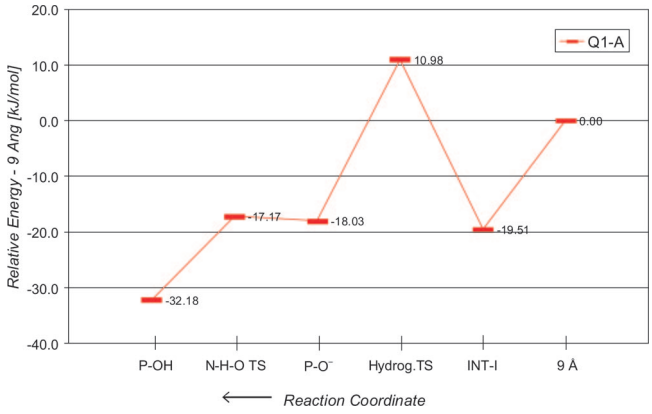

Figure 16. Potential energy surface for the hydrogen transfer cyclohexyl methyl ketone−cyclohexyl methyl alcohol reaction catalysed by *trans*-Ru(H)$_2$(*S*,*S*-dpen)(*S*-xylbinap) along the Q1-**B** pathway, as computed by the DFT-PBE method.

Å for Q1-**A**, Q1-**B**, Q2-**A**, Q2-**B**, and Q3-**B** have been freely optimized. The energetics and optimized stuctures of the intermediate (INT-I) and the transition state (Hydrog.TS) structures associated with Q1, Q2, and Q3 are described in Table 3 and shown in Figure 15. The energies of INT-I, Hydrog.TS, and separated reactants (taken at 9 Å) associated with the Q1-A approach have also been evaluated at the MPWB1K level.[28] The relative energies obtained using MPWB1K ($\Delta E_{\text{Hydrog.TS}} = 7.60$ kJ/mol, $\Delta E_{\text{INT-I}} = -21.75$ kJ/mol) are in reasonable agreement with the PBE results ($\Delta E_{\text{Hydrog.TS}} = 10.98$ kJ/mol, $\Delta E_{\text{Q1-A}} = -19.51$ kJ/mol).

From the relative energies reported in Table 4, it is possible to deduce that the reaction will proceed through the reaction pathways Q1-**A**, Q1-**B**, and Q2-**B**. In fact, the activation barriers for the H-transfer cyclohexyl methyl ketone-cyclohexyl methyl alcohol reaction along Q1 and Q2-**B** ($\Delta E^{a}_{\text{Q1-A}} = 30.49$ kJ/mol; $\Delta E^{a}_{\text{Q1-B}} = 30.42$ kJ/mol; $\Delta E^{a}_{\text{Q2-B}} = 33.19$ kJ/mol) are considerably lower than the activation energies for Q2-**A** and Q3-**B** ($\Delta E^{a}_{\text{Q2-A}} = 40.63$ kJ/mol; $\Delta E^{a}_{\text{Q3-B}} = 47.78$ kJ/mol). As regards the binding energy, the comparison of Q1 ($\text{BE}_{\text{Q1-A}} = -19.51$ kJ/mol, $\text{BE}_{\text{Q1-B}} = -17.92$ kJ/mol) and Q2-**B** ($\text{BE}_{\text{Q2-B}} = -17.86$ kJ/mol) indicates that the binding-recognition step for [**1** + cyclohexyl methyl ketone] is also not very effective for the differentiation of the two prochiral faces of the cyclohexyl methyl ketone. Therefore, we explain the low enantioselectivity experimentally observed for the *trans*-Ru(H)$_2$(*S*,*S*-dpen)(*S*-xylbinap)-catalyzed hydrogenation of cyclohexyl methyl ketone[14] in terms of lack of kinetic (with ΔE^{a} similar for Q1 and Q2-**B**) and thermodynamic factors (with BE similar for Q1 and Q2) which can differentiate the two prochiral faces of the ketone.

Stereoselectivity requires effective differentiation between two alkyl groups. For acetophenone, it has been shown that for [**1** + acetophenone] ΔBE(Q1−Q2) = 5.51 kJ/mol (see Table 2), while for [**2** + acetophenone] ΔBE(Q1−Q2) = 4.71 kJ/mol (see Table 3). On the other hand, for [**1** + cyclohexyl methyl ketone] ΔBE(Q1−Q2) is just 1.65 kJ/mol. The reason for this difference can be understood by comparing the INT-I structures along the Q1-**B** and Q2-**B** approaches (see Figure 15). It is possible to observe that in both approaches of the ketone, the cyclohexyl group, which

is in the "chair" conformation, points upward and away from the pocket made by the bulky aryl groups of the ligands. Consequently, there is no differentiation of the two alkyl groups. For example, the minimum H···H distances computed for the intermediate along Q1-**B** (2.350 and 2.449 Å in Figure 15) are very similar to the minimum H···H distances reported for the intermediate along Q2 (2.379 and 2.439 Å in Figure 15). On the other hand, it has been shown in section 3.1 that for the system [**1** + acetophenone] the differentiation of the phenyl and methyl group comes from the occurrence along the Q1 approach of stronger X−H/π hydrogen bond interactions and weaker steric H···H effects.

In Figure 16, the PES for the H-transfer cyclohexyl methyl ketone-cyclohexyl methyl alcohol catalyzed by **1** along the Q1-**B** approach. Note that for Q1-**B**, the Hydrog.TS corresponds to the fully optimized transition state structure (see section 2.1 and Table 5). Also for the system [**1** + cyclohexyl methyl ketone], our calculations suggest that in the gas-phase the H-transfer occurs through a stepwise mechanism: transfer of (Ru−)H hydride to the C(═O) followed by (N−)H donation to the O.

4. Summary and Conclusions

This study has reported detailed gas-phase DFT-PBE calculations on real-size systems [*trans*-Ru(H)$_2$(*S*,*S*-dpen)(*S*-xylbinap) + acetophenone], [*trans*-Ru(H)$_2$(*S*,*S*-dpen)(*S*-tolbinap) + acetophenone], and [*trans*-Ru(H)$_2$(*S*,*S*-dpen)(*S*-xylbinap) + cyclohexyl methyl ketone]) in order to identify the factors controlling the enantioselectivity in Ru(diphosphine)(diamine) catalysts. Particular emphasis has been given to the rationalization of the meta-dialkyl effect, which is observed in the hydrogenation of acetophenone when the reaction is catalyzed by *trans*-Ru(H)$_2$(*S*,*S*-dpen)(*S*-xylbinap) and *trans*-Ru(H)$_2$(*S*,*S*-dpen)(*S*-tolbinap), and to understanding the factors that determine the low performance of Ru(diphosphine)(diamine) catalysts for the enantioselective hydrogenation of aliphatic ketones.

The DFT-PBE results suggest that the meta-dialkyl effect in the *trans*-Ru(H)$_2$(*S*,*S*-dpen)(*S*-xylbinap)-catalyzed acetophenone hydrogenation is connected with the formation of a very stable intermediate (INT-II) along the Q1 reaction pathway, which gives the *R*-alcohol as a resulting product, where the acetophenone has the same conformation as in the Hydrog.TS structure. The extra-stabilization of INT-II has been explained in terms of XH/π [X = C(sp^2) and N] hydrogen bond like attractive interactions which occur when the reactant enters the catalyst pocket fixing the molecular conformation. The formation of this intermediate is hindered for the competitive pathways. For the Q2 approach, we have demonstrated that the steric interaction between the methyl groups (in the meta position with respect to the phosphorus atom) of the diphosphine ligand and the phenyl group of the acetophenone forces a drastic torsion of the phenyl group on going from the reactant-complex to the transition state structure. The additional energy associated with the rotation of the phenyl group makes the Q2 approach (*S*-product) considerably more unfavorable than the Q1 approach (*R*-product).

For the *trans*-Ru(H)$_2$(*S*,*S*-dpen)(*S*-tolbinap)-catalyzed acetophenone hydrogenation reaction, the absence of methyl groups in the meta position with respect to the phosphorus atoms of the diphosphine ligand allows for the formation of a single intermediate along the competitive (Q1, Q2) reaction pathways, where the acetophenone is already in the same conformation as in the transition state structure. Consequently, there is no kinetic factor which differentiates the two prochiral faces of the acetophenone ($\Delta E^a_{Q1} \approx \Delta E^a_{Q2}$). The calculation of the binding energies associated with the approach of the ketone along Q1 and Q2 suggests that the reaction is driven through the (*R*)-product simply by the binding process ($BE_{Q1} > BE_{Q2}$).

Finally, the results on the *trans*-Ru(H)$_2$(*S*,*S*-dpen)(*S*-xylbinap)-catalyzed hydrogenation of cyclohexyl methyl ketone indicate that the low enantioselectivity observed for this reaction is due to the absence of kinetic and thermodynamic factors differentiating the two prochiral faces of the ketone. With regard to the differentiation between the two alkyl groups as the cyclohexyl methyl ketone approaches to the catalyst, we have shown that the particular conformation of the cyclohexyl group (chair conformation) does not allow for a specific differentiation of the two alkyl groups during the binding recognition process.

Acknowledgment. This work is partially funded by the Department of Trade and Industry's "Manufacturing Molecules Initiative" with contributions from Astrazeneca, GlaxoSmithKline, Johnson Matthey and Pfizer. Additional support has been provided by the EPSRC Portfolio Partnership grant EP/D504872. Dr. Alexey Sokol, Prof. Jianliang Xiao, and Dr. Andreas Danopoulos are thanked for useful discussions.

IC701981V